Ann. Rev. Nucl. Part. Sci. 1983. 33:611–44

INTERNAL SPIN STRUCTURE OF THE NUCLEON

Vernon W. Hughes

Physics Department, Yale University, New Haven, Connecticut 06520

Julius Kuti

Institute for Theoretical Physics, University of California, Santa Barbara, California 93106

CONTENTS

1. INTRODUCTION

The study of the structure of the proton and neutron through deep inelastic scattering, initially with electrons but subsequently with muons and neutrinos as well, has played a central role in establishing the quark-parton theory of the composition of hadrons and of quantum chromodynamics (QCD). One important aspect of these theoretical and experimental developments is the two spin-dependent structure functions, which are independent of the two spin-averaged structure functions and define the internal spin structure of the nucleon.

Since both quarks and gluons possess spin and the forces between them are spin dependent, we can expect important information on these forces and on nucleon structure to be obtained through the study of the spin-dependent aspects of the nucleon wave function, as has been the case before in atomic and nuclear physics. The deep inelastic polarization experiment

0163-8998/83/1201-0611$02.00

probes the spin distribution of quark constituents inside the nucleon. The theoretical description is expected to come from QCD.

Quantum chromodynamics—the theory of colored quarks and gluons and their interactions—is the presently accepted theory of strong interactions (1–4). Just as for the spin-independent structure functions, QCD predicts certain general sum rules and scaling behavior for the spin-dependent structure functions, whose verification can provide important confirmation of theory.

The hadronic currents of the electromagnetic and weak interactions are built from bilinear expressions of local quark fields providing a mathematical and physical relation between electromagnetic and weak hadronic phenomena. In the years before QCD emerged as the leading candidate for the theory of strong interactions, the quark-parton model had an elegant formulation in terms of the algebra of hadron currents (5–8). It was assumed that the product of two local hadronic currents with light-like separation between them was calculable as though the quark fields obeyed the free Dirac equation on the light cone. The scaling prediction for the spin-averaged and spin-dependent structure functions was an immediate consequence of this assumption (quark light-cone algebra). The scaling functions had a direct interpretation in terms of quark and gluon distributions inside the nucleon. The sum rules of the quark-parton model were elegant consequences of the quark light-cone algebra.

Quantum chromodynamics provides a theoretical explanation and a physical picture of why the interaction between quarks and gluons would vanish asymptotically at very short distances. This perturbative QCD supports the assumptions of the quark light-cone algebra and the quark-parton model. Even more powerfully, as a theory should predict new things, it describes quantitatively the logarithmic rate at which quarks become asymptotically free at short distances (9, 10).

The logarithmic corrections to the scaling functions and sum rules are the most important new predictions of perturbative QCD. In particular, the scaling behavior of spin-dependent structure functions and the corrections to it are accurately predicted in QCD together with some important sum rules of the scaling functions.

The calculation of the quark spin distributions inside the nucleon is a difficult nonperturbative calculation. As yet it has not been possible to calculate spin-dependent (or spin-independent) structure functions from the basic equations of QCD. However, models of nucleon structure have been developed consistent with the general picture of QCD, which make quantitative predictions of the structure functions. In atomic and nuclear physics it has often been found that spin-dependent observables provide particularly sensitive tests of a system's wave function, and we may

anticipate that for the nucleon also spin-dependent quantities will be illuminating. We may remark that an enormous theoretical literature on the spin-dependent structure functions of the nucleon has developed since about 1970.

Information about the spin-dependent structure functions of the nucleon requires the measurement of spin-dependent asymmetrics in the deep inelastic scattering of high energy polarized electrons (or muons) from polarized nucleons (11). The measured asymmetry A compares the cross sections for the case of parallel and antiparallel spins of the colliding particles and is given by

$$A = \frac{d\sigma^{\uparrow\downarrow} - d\sigma^{\uparrow\uparrow}}{d\sigma^{\uparrow\downarrow} + d\sigma^{\uparrow\uparrow}} \qquad 1.$$

where $d\sigma^{\uparrow\uparrow}$ is the cross section when the spins of electron and proton are parallel and along the direction of motion of the incident electron; $d\sigma^{\uparrow\downarrow}$ is the cross section for antiparallel spins. The measurements are made for inclusive scattering so that the momentum and scattering angle of the outgoing electron is observed but the final state of the proton is not detected. Since the technologies of polarized electron sources and polarized nucleon targets are difficult and also limiting with respect to intensity and polarization, relatively few data are available on the spin-dependent structure functions as compared to the data that have been obtained on spin-independent structure functions. Indeed, experiments at SLAC on polarized e-p scattering of longitudinally polarized electrons by longitudinally polarized protons provide our only experimental information to date.

The theory of polarized e-p scattering in leading order of the fine structure constant α is based on the exchange of a single virtual photon between the electron and the nucleon. Since the hadronic final state is not detected in the experiment, the spin-dependent differential cross section of the scattering is proportional to the antisymmetric part of the hadronic tensor amplitude $W_{\mu\nu}(Q^2, \nu)$, which is completely determined in terms of two spin-dependent structure functions $G_1(Q^2, \nu)$ and $G_2(Q^2, \nu)$. The terms Q^2 and ν are the relativistic invariants of four-momentum transfer to the nucleon and of energy loss by the electron, respectively.

The spin-dependent structure functions appear in the numerator of virtual photon-nucleon asymmetries $A_1(Q^2, \nu)$ and $A_2(Q^2, \nu)$. The asymmetry A_1 is the quantity measured thus far in polarized e-p scattering and it is given by

$$A_1 = \frac{\sigma_{1/2} - \sigma_{3/2}}{\sigma_{1/2} + \sigma_{3/2}} \qquad 2.$$

where $\sigma_{1/2}$ and $\sigma_{3/2}$ are the virtual photon-nucleon absorption cross

sections when the projection of total angular momentum of virtual photon plus nucleon along the virtual photon direction is 1/2 and 3/2, respectively.

There is an important general sum rule related to the spin-dependent structure functions—the Bjorken polarization sum rule—which is given in its scaling form by the integral (12–17)

$$2\int_0^1 [g_1^p(x) - g_1^n(x)]\, dx = \frac{1}{3}\left|\frac{g_A}{g_V}\right|, \qquad 3.$$

where g_A/g_V is the ratio of axial to vector weak coupling constants in nucleon beta decay. The limiting scaling function as derived from $G_1(Q^2, \nu)$ is designated by $g_1(x)$. It has a remarkable and simple physical interpretation (18) in terms of quark spin distributions in the quark-parton model,

$$g_1(x) = \frac{1}{2}\sum_i e_i^2 [f_i^{\uparrow}(x) - f_i^{\downarrow}(x)], \qquad 4.$$

where $f_i^{\uparrow}(x)$ and $f_i^{\downarrow}(x)$ are interpreted as the probabilities of finding a quark parton of type i in a fast moving longitudinally polarized nucleon with a fraction x of the nucleon total momentum and with spin projected along or opposite to the nucleon spin, respectively. The charge e_i of the quark is measured in electron charge units. The Bjorken polarization sum rule involves the difference of scaling functions for protons and neutrons. The variable x is also the scaling variable $x = Q^2/2M\nu$ in the deep inelastic limit where x is fixed and Q^2, $\nu \to \infty$. The quark-parton picture is valid only in this limit (19–21).

The remarkable relation in Bjorken's sum rule between scaling functions in polarized deep inelastic electron scattering and the nucleon beta decay, which is a low energy phenomenon, is explained by the free light-cone behavior of the quark fields. The hadronic tensor amplitude is given by the commutator of the hadronic part of the electromagnetic current sandwiched between identical proton states. The two currents in the commutator are separated by light-like distances for the dominant contribution to deep inelastic scattering. The commutator is calculable there in terms of free quark fields and reduced to an axial vector current with calculable SU(3) flavor structure. This axial vector matrix element relates to nucleon beta decay for the proton-neutron difference on the right-hand side.

The Bjorken sum rule is a rigorous consequence of QCD in the limit $Q^2 \to \infty$. QCD also predicts the leading correction to the sum rule for finite Q^2 in terms of the strong interaction coupling constant α_s (22–25).

The quark-parton theory of nucleon structure makes a general qualitative prediction that one of the spin-dependent asymmetries A_1 for the proton is positive. Current phenomenological models of nucleon structure based on the quark-parton model predict values of the spin-dependent nucleon structure functions. The measured large positive asymmetry is against the

early simple bootstrap picture of the nucleon. In the bootstrap model the nucleon was the bound state of a nucleon and a pion in P-orbital wave. This angular momentum structure would produce a large negative asymmetry A_1 ruled out by the Yale-SLAC data (26). Although the structure functions cannot be calculated yet from the basic QCD Hamiltonian, perturbative QCD predicts that at large x near to one, $A_1 \simeq 1$ for both proton and neutron, i.e. a quark (either u or d) that carries a large fraction of the momentum of the nucleon also carries the nucleon's spin (27–29).

The data obtained on polarized e-p scattering (11) determine the spin-dependent structure function A_1 of the proton over the deep inelastic kinematic range $0.1 < x < 0.7$ and $1 < Q^2 < 10\,(\mathrm{GeV}/c)^2$ with accuracy of 15–30%. There are also some data for elastic scattering and for resonance-region scattering (27).

The experimental data do confirm the Bjorken polarization sum rule at the parton-quark level (31) under the assumption that the neutron contributes a negligible amount; the data also verify the scaling behavior of A_1^p within their limited accuracy. Furthermore the data successfully distinguish the phenomenological models of the internal spin structure of the proton, as well as support the prediction of perturbative QCD that $A_1^p(x) \to 1$ as $x \to 1$.

We should also mention here an interesting connection between polarized electron-proton scattering and the hyperfine splitting in atomic hydrogen. The hyperfine splitting of the hydrogen ground state may receive an appreciable contribution from the proton's polarizability by the orbiting electron (12, 32–34). This contribution is directly calculable from the spin-dependent structure functions $G_1(Q^2, \nu)$ and $G_2(Q^2, \nu)$. This information would provide an exceptional bridge between quark physics of short distances and high precision atomic physics.

The possibilities of obtaining additional experimental information on the spin-dependent structure functions both with polarized electron and polarized muon beams are excellent. Additional data will allow exciting comparisons to be made with the many theoretical predictions. Perhaps the most outstanding quantitative prediction at present is the Bjorken polarization sum rule. Its reliable measurement would require data on polarized neutron (polarized deuteron) scattering which remains the most important experiment project for the future in the field of polarized electron (muon)-nucleon scattering.

2. THEORY

We review here the theoretical significance of inelastic scattering of polarized electrons from polarized nucleons (35, 36). The Feynman diagram that describes the scattering process in leading order of the electromagnetic

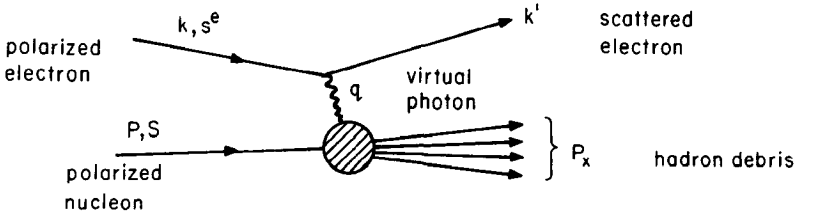

Figure 1 The Feynman diagram of spin-dependent deep inelastic electron-nucleon scattering in the one-photon exchange approximation.

coupling is shown in Figure 1. The polarized electron emits a virtual photon of four-momentum q which is absorbed by the polarized nucleon target. The nucleon explodes into some hadron debris that is not detected in the experiment.

The incoming electron is characterized by its four-momentum k and polarization four-vector S^e. The polarization state of the scattered electron is summed in the experiment. The target nucleon has four-momentum P and its polarization four-vector is S. The polarization vector S is reduced to the nucleon's spin three-vector $\mathbf{S}$, $S = (0, \mathbf{S})$ in the target rest frame.

The relativistic invariants,

$$-q^2 = Q^2 = -(k-k')^2 = 4EE' \sin^2 \frac{\theta}{2},$$

$$\nu = \frac{P \cdot Q}{M} = E - E', \qquad 5.$$

$$W^2 = (P+q)^2 = M^2 + 2M\nu - Q^2,$$

are well-known from spin-averaged deep inelastic lepton-nucleon scattering. In Equation 5, M designates the nucleon mass; E and E' are the incoming and outgoing electron energies, respectively. The laboratory scattering angle of the electron is θ. The deep inelastic limit of the scattering process is defined by the kinematic conditions $Q^2 \gg M^2$ and $W \gg M$.

The inelastic cross section in the laboratory is given by

$$\frac{d^2\sigma^{S_e S}}{d\Omega\, dE'} = \frac{4\alpha^2}{Q^4} \frac{E'}{E} L_{\mu\nu} W^{\mu\nu}, \qquad 6.$$

where α is the fine structure constant and $d\Omega$ designates the differential solid angle of the scattered electron with respect to the beam. The lepton current is described by the tensor $L_{\mu\nu}$, which is split into the sum of a polarization-independent symmetric part and a polarization-dependent antisymmetric part,

$$L_{\mu\nu} = k'_\mu k_\nu + k'_\nu k_\mu - g_{\mu\nu} k' \cdot k + i m_e \varepsilon_{\mu\nu\alpha\beta} S_e^\alpha q^\beta, \qquad 7.$$

after summation over the polarization of the scattered electron. The metric is defined by $g_{00} = -g_{11} = -g_{22} = -g_{33} = +1$, and $\varepsilon_{\mu\nu\alpha\beta}$ designates the completely antisymmetric tensor in the four indices μ, ν, α, and β with $\varepsilon_{\mu\nu\alpha\beta} = +1$ for even permutations of 1234. For longitudinally polarized electrons the polarization four-vector S^e in the laboratory system is $S^e = 1/m_e(k, 0, 0, E)$ so that the electron mass m_e in the spin-dependent part of $L_{\mu\nu}$ cancels.

The tensor for the longitudinally polarized lepton is characterized by the parameter ε,

$$\varepsilon = \left[1 + 2\left(1 + \frac{\nu^2}{Q^2}\right)\tan^2\frac{\theta}{2}\right]^{-1}, \qquad 8.$$

which is the ratio of the longitudinally to the transversely polarized virtual photon fluxes.

The hadronic tensor amplitude $W_{\mu\nu}$ also has a decomposition into the sum of of a symmetric spin-independent part and an antisymmetric spin-dependent part,

$$W_{\mu\nu} = W^S_{\mu\nu} + iW^A_{\mu\nu} = \frac{1}{2\pi}\int d^4x\, e^{iqx}\langle P, S|[J_\mu(x), J_\nu(0)]|P, S\rangle, \qquad 9.$$

where $J_\mu(x)$ designates the hadronic electromagnetic current. The spin-independent symmetric part defines the well-known spin-independent structure functions $W_1(Q^2, \nu)$ and $W_2(Q^2, \nu)$,

$$W^{\mu\nu}_S = \left(-g^{\mu\nu} + \frac{q^\mu q^\nu}{q^2}\right)W_1 + \frac{1}{M^2}\left(P^\mu - \frac{P\cdot q}{q^2}q^\mu\right)\left(P^\nu - \frac{P\cdot q}{q^2}q^\nu\right)W_2. \qquad 10.$$

The antisymmetric tensor amplitude defines the spin-dependent structure functions $G_1(Q^2, \nu)$ and $G_2(Q^2, \nu)$,

$$W^{\mu\nu}_A = M\varepsilon^{\mu\nu\alpha\beta}q_\alpha S_\beta G_1 + \frac{1}{M}\varepsilon^{\mu\nu\alpha\beta}q_\alpha[(P\cdot q)S_\beta - (S\cdot q)P_\beta]G_2. \qquad 11.$$

The measured asymmetry A in the Yale-SLAC experiments compares the cross sections for the case of parallel and antiparallel spin of the colliding particles, and is defined by

$$A = \frac{d\sigma^{\uparrow\downarrow} - d\sigma^{\uparrow\uparrow}}{d\sigma^{\uparrow\downarrow} + d\sigma^{\uparrow\uparrow}}, \qquad 12.$$

where $d\sigma^{\uparrow\uparrow}$ is the cross section when the spins of electron and proton are parallel and along the direction of motion of the incident electron; $d\sigma^{\uparrow\downarrow}$ is the cross section for antiparallel spins.

The spin dependence of the differential cross sections in terms of the spin-

dependent structure function is given by

$$\frac{d^2\sigma^{\uparrow\downarrow}}{d\Omega\, dE'} - \frac{d^2\sigma^{\uparrow\uparrow}}{d\Omega\, dE'} = \frac{4\alpha^2}{Q^2}\frac{E'}{E}[M \cdot G_1(E + E' \cos\theta) - Q^2 G_2]. \quad 13.$$

It is also useful to define virtual photon-nucleon asymmetries, A_1 and A_2, given by

$$A_1 = \frac{\sigma_{1/2} - \sigma_{3/2}}{\sigma_{1/2} + \sigma_{3/2}}, \quad 14.$$

$$A_2 = \frac{\sigma_{TL}}{\sigma_T}, \quad 15.$$

where $\sigma_{1/2}$ and $\sigma_{3/2}$ are the total virtual photoabsorption cross sections when the projection of total angular momentum of virtual photon plus nucleon along the virtual photon direction is 1/2 and 3/2, respectively. The cross section σ_T is defined by the relation $\sigma_T = 1/2(\sigma_{1/2} + \sigma_{3/2})$, and σ_{TL}, which may be negative, is a term arising from the interference between transverse and longitudinal photon-nucleon amplitudes.

The asymmetry A in Equation 12 relates to A_1 and A_2 by

$$A = D(A_1 + \eta A_2), \quad 16.$$

where

$$D = \frac{1 - (E'/E)\varepsilon}{1 + \varepsilon R} \quad 17.$$

can be regarded as a kinematic depolarization factor of the virtual photon. The quantity $R = \sigma_L/\sigma_T$ is the ratio of longitudinal and transverse virtual photoabsorption cross sections. The kinematic factor η is given by

$$\eta = \varepsilon(Q^2)^{1/2}/(E - E'\varepsilon). \quad 18.$$

There are some rigorous positivity limits (15, 16, 37, 38) imposed on A_1 and A_2:

$$|A_1| \leq 1, \qquad |A_2| \leq \sqrt{R} \quad 19.$$

The asymmetries A_1 and A_2 can be written in terms of spin-dependent structure functions

$$A_1 = \frac{M\nu G_1 - Q^2 G_2}{W_1} \quad 20.$$

$$A_2 = \frac{\sqrt{Q^2}}{W_1}(MG_1 + \nu G_2). \quad 21.$$

We turn now to the most important properties of the spin-dependent structure functions. One can take the scaling limit where $\nu, Q^2 \to \infty$ with $x = Q^2/2M\nu$ fixed. In that limit the light-cone behavior of the electromagnetic current commutator in Equation (9) dominates the hadronic tensor amplitude. Since $J_\mu(x)$ is built from local quark fields, the scaling limit is governed by the quark light-cone algebra of the hadronic currents (15–17).

It follows from the leading singularities of the quark light-cone commutators through Fourier transformation that

$$M^2\nu G_1(Q^2, \nu) \to g_1(x) \qquad 22.$$

and

$$M\nu^2 G_2(Q^2, \nu) \to g_2(x) \qquad 23.$$

in the scaling limit. This scaling behavior of the spin-dependent structure functions is a rigorous consequence of the short-distance properties of QCD, since the quark light-cone algebra itself follows from the short distance part of QCD. Equations 22 and 23 are actually modified by logarithmic corrections in Q^2 in the rigorous derivation from QCD. Those corrections will appear manifestly in important sum rules for the spin-dependent structure functions.

The scaling functions $g_1(x)$ and $g_2(x)$ have direct physical interpretations in terms of quark partons (18, 21, 39). The following relations are valid in the quark-parton model.

$$g_1(x) = \frac{1}{2}\sum_i e_i^2[f_i^{\uparrow}(x) - f_i^{\downarrow}(x)], \qquad 24.$$

$$g_1(x) + g_2(x) = \frac{1}{2Mx}\sum_i e_i^2 m_i[f_i^{T\uparrow}(x) - f_i^{T\downarrow}(x)]. \qquad 25.$$

Here $f_i^{\uparrow}(x)$ and $f_i^{\downarrow}(x)$ are interpreted as the probabilities of finding a quark parton of type i in a longitudinally polarized nucleon with a fraction x of the nucleon total momentum and with spin projected along or opposite to the nucleon spin, respectively. The charge of the ith quark parton is measured in electron charge units and designated by e_i. The sum runs over all quark types.

The other quark spin distribution functions $f_i^{T\uparrow}(x)$ and $f_i^{T\downarrow}(x)$ have a slightly more complicated physical interpretation. They refer to a situation where the nucleon and the quark partons are polarized in the transverse direction.

The second relation in Equation 25 relates to the asymmetry A_2 as

$$\frac{\nu}{\sqrt{Q^2}} A_2 \xrightarrow[\substack{\nu, Q^2 \to \infty \\ x \text{ fixed}}]{} \frac{g_1(x)+g_2(x)}{F_1(x)} \qquad 26.$$

in the above discussed scaling limit, where

$$F_1(x) = \frac{1}{2}\sum_i e_i^2 [f_i^{\uparrow}(x)+f_i^{\downarrow}(x)]. \qquad 27.$$

It is shown that, in the approximation in which the quark partons are on their mass shell without transverse momenta, the second structure function $g_2(x)$ vanishes. The asymmetry A_2 is proportional to the quark masses m_i through Equations 25 and 26. Therefore, A_2 would vanish for massless quarks.

The asymmetry A_1 is the dominant term in deep inelastic scattering with longitudinal polarization. It has a very simple and transparent physical interpretation in the scaling limit,

$$A_1(x) = \frac{\sum_i e_i^2 [f_i^{\uparrow}(x)-f_i^{\downarrow}(x)]}{\sum_i e_i^2 [f_i^{\uparrow}(x)+f_i^{\downarrow}(x)]} \qquad 28.$$

if $R \to 0$ in the same limit as predicted from the quark-parton picture, or, more generally, from the short-distance behavior of QCD.

The most important sum rule for spin-dependent deep inelastic electron-nucleon scattering was derived first by Bjorken from the commutator algebra of hadronic currents with underlying quark fields. At that time the theoretical scaling behavior of the spin-dependent structure functions was not known yet. Knowing now the scaling behavior of $G_1(Q^2, \nu)$, the sum rule for the difference of $g_1(x)$ for protons and neutrons is

$$2\int_0^1 [g_1^p(x)-g_1^n(x)]\, dx = \frac{1}{3}\left|\frac{g_A}{g_V}\right| = 0.418 \pm 0.002 \qquad 29.$$

where g_A/g_V is the ratio of axial to vector weak coupling constants in nucleon beta decay.

The scaling form of Bjorken's sum rule in Equation 29 can be rewritten in a form

$$\int_0^1 \frac{dx}{x}\left[\frac{A_1^p(x)F_2^p}{1+R^p} - \frac{A_1^n(x)F_2^n(x)}{1+R^n}\right] = \frac{1}{3}\left|\frac{g_A}{g_V}\right| \qquad 30.$$

that is convenient for the experimental analysis. The scaling function $F_2(x)$ is the scaling limit of νW_2. The sum rule is valid in the scaling limit where R

$= 0$, but is convenient to keep R in Equation 30 for comparison with finite Q^2 data where $R \neq 0$ is known from the spin-independent experiment.

Separate sum rules were derived (40) from the quark light-cone algebra for protons and neutrons under the assumption that the net spin polarization of strange sea quarks is zero:

$$2\int_0^1 g_1^p(x)\,dx = \int_0^1 \frac{dx}{x}\frac{A_1^p(x)F_2^p(x)}{1+R^p} = \left|\frac{g_A}{g_V}\right|\frac{0.89}{3} = 0.372 \pm 0.002, \qquad 31.$$

and

$$2\int_0^1 g_1^n(x)\,dx = \int_0^1 \frac{dx}{x}\frac{A_1^n(x)F_2^n(x)}{1+R^n} = \left|\frac{g_A}{g_V}\right|\frac{(-0.11)}{3} = -0.046 \pm 0.0002. \qquad 32.$$

There exist data now to test the sum rule in Equation 31. The neutron sum rule should be tested in future experiments.

The scaling form of the Bjorken sum rule is not strictly valid in quantum chromodynamics. The quark-gluon coupling constant is approaching zero with increasing Q^2 in QCD. Therefore the quark partons become free only asymptotically when $Q^2 \to \infty$ and the structure functions receive logarithmic Q^2 corrections from quark-gluon and gluon-gluon interactions. The running coupling constant has the form (4, 8)

$$\alpha_s(Q^2) = \frac{1}{c\,\ln(Q^2/\Lambda^2)} \qquad 33.$$

where double logarithmic corrections are neglected. The constant c in Equation 33 is calculable theoretically,

$$c = \frac{33-2f}{12\pi} \qquad 34.$$

where f is the number of quark flavors. The scale parameter Λ sets the strength of quark-gluon coupling in QCD. With careful definition of the neglected corrections (69) in Equation 33, the experimental value of Λ is somewhere around 100 MeV from deep inelastic scattering and e^+e^- annihilation.

The effect of asymptotic freedom on the Bjorken sum rule is an additive Q^2 dependent correction (22):

$$\int_0^1 dx\,[g_1^p(x) - g_1^n(x)] = \frac{1}{6}\left|\frac{g_A}{g_V}\right|\left(1 - \frac{\alpha_s(Q^2)}{\pi}\right), \qquad 35.$$

where the running coupling constant $\alpha_s(Q^2)$ is given in Equation 33.

A sum rule also for the second spin-dependent structure function G_2

follows from angular momentum conservation. The sum rule for protons or neutrons (17, 18, 41) is

$$\int_0^1 g_2(x)\,dx = 0 \qquad 36.$$

in the scaling limit. There are some subtleties about the convergence of the integral in Equation 36 that we do not discuss here (42).

Scaling of the structure functions, the Bjorken sum rule, and asymptotic freedom corrections to the scaling limit are accurate predictions from the short-distance behavior of QCD. The calculation of the quark spin distributions inside the nucleon is a more difficult task. It would require the nonperturbative calculation of the nucleon structure in terms of quark and gluon wavefunctions. There is an exciting new development in QCD which treats that difficult problem from the numerical point of view using stochastic methods and computer simulation (43). Though the first nonperturbative results are very interesting they do not yield enough information yet on the quark and gluon distributions inside the nucleon. We have to turn, therefore, to somewhat more model-dependent descriptions.

We estimate first the asymmetry A_1 in a very simple quark model where the SU(6) quarks are identified with the partons scattering the incoming polarized electrons. The static wave function of the proton with spin up is given by

$$\begin{aligned}|\text{proton}\uparrow\rangle = \frac{1}{\sqrt{18}}(&2|u^\uparrow d^\downarrow u^\uparrow\rangle + 2|u^\uparrow u^\uparrow d^\downarrow\rangle + 2|d^\downarrow u^\uparrow u^\uparrow\rangle \\ &- |u^\uparrow u^\downarrow d^\uparrow\rangle - |u^\uparrow d^\uparrow u^\downarrow\rangle - |u^\downarrow d^\uparrow u^\uparrow\rangle \\ &- |d^\uparrow u^\downarrow u^\uparrow\rangle - |d^\uparrow u^\uparrow u^\downarrow\rangle - |u^\downarrow u^\uparrow d^\uparrow\rangle).\end{aligned} \qquad 37.$$

The probability of interaction with a $u^\uparrow$ quark (spin up) is 5/9, and with a $u^\downarrow$ quark it is 1/9 according to the spin wave function in Equation 37. The corresponding probabilities for $d^\uparrow$ and $d^\downarrow$ quarks are 1/9 and 2/9, respectively.

The asymmetry A_1 is given by simple counting (12). Only quarks with spin antiparallel to the spin of the virtual photon contribute, and the cross section is proportional to (charge)^2. Quarks with spin $+1/2$ contribute to $\sigma_{1/2}$ and we find $\sigma_{1/2} = 21/81$. Quarks with spin $-1/2$ contribute to $\sigma_{3/2}$ with $\sigma_{3/2} = 9/81$. This leads to an asymmetry $A_1 = 5/9$. From isospin symmetry the prediction for the neutron is $A_1 = 0$.

This simple picture has to be modified in various aspects. In the limit $x \to 0$ the electron is scattered by quarks in the $q\bar{q}$ "sea" decoupled from the

proton's spin. We expect the asymmetry A_1 to vanish in this limit. In the other extreme limit $x \to 1$, one quark carries the proton's momentum. With its spin parallel to the proton's it gives $A_1 = 1$ in that limit.

A simple quark-parton model was proposed with some modifications to incorporate the expected qualitative features of quark and gluon distributions inside the nucleon (18, 39, 44–50). This simple quark-parton model picture which has emerged during the years describes the observed asymmetry $A_1(x)$ both in shape and magnitude.

The quark-parton models of spin-dependent structure functions emerged from the unification of the spin-isospin wave function of the SU(6) quark model and of Feynman's parton picture. The calculation of structure functions in the MIT bag model proceeds in a different fashion (51). Relativistic quarks are confined inside the nucleon by vacuum pressure and the structure functions are calculated in the rest frame of the nucleon from the light-cone behavior of the hadronic currents.

There was also some attempt to describe the spin-dependent structure functions in terms of direct channel resonance excitations (52–54). General sum rules were proposed as a spin-dependent electroproduction test of relativistic constituent quarks (55).

There is a very interesting side application of polarized deep inelastic electron-proton scattering for the hyperfine splitting in atomic hydrogen. This is an exceptional bridge between the usually disconnected fields of high energy quark physics and high precision atomic physics.

One finds a contribution δ_{pol} to the hyperfine splitting of the hydrogen ground state (56) from the Feynman diagram of Figure 2. This diagram has an unknown part in it that is the spin-dependent Compton scattering amplitude of a virtual photon on the proton. The diagram with a loop integral describes the proton polarizability contribution to the hyperfine splitting. Through dispersion relations the virtual Compton amplitude in Figure 2 relates to the spin-dependent structure functions G_1 and G_2.

Our partial knowledge of the properties of the structure functions G_1 and

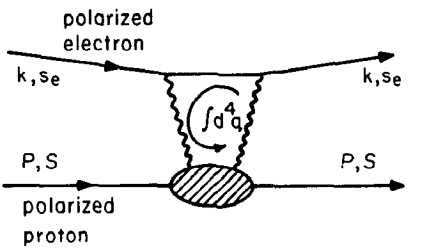

Figure 2 The Feynman diagram of the proton's polarizability contribution to the hyperfine splitting of the hydrogen ground state.

G_2, together with rigorous inequalities, puts limits on the polarization contribution (33, 34)

$$-4 \text{ ppm} \leq \delta_{\text{pol}} \leq 4 \text{ ppm}. \qquad 38.$$

Further information on G_1 and G_2 would make it feasible to actually calculate δ_{pol} completing this nice bridge between high energy quark physics and low energy, high precision atomic physics.

3. EXPERIMENT

As discussed in Section 2, determination of the spin-dependent structure functions of the nucleon requires the use of a high energy polarized electron (or muon) beam and of a polarized proton (or neutron) target to measure spin-dependent asymmetries in the inclusive scattering $e^- + p \rightarrow e^- + X$ (unobserved). Thus far, data have been obtained only for the scattering of longitudinally polarized electrons by longitudinally polarized protons (Equation 16).

3.1 *Polarized Electron Beam*

There are many possible schemes for producing polarized electrons (57). The polarized electron source that was developed at Yale and used in the high energy e-p polarization experiment at SLAC was an atomic beam source based on the photoionization of electron spin polarized, lithium-6 atoms (58, 59). A diagram of the energy levels and magnetic moments for the ground $^2S_{1/2}$ state of ^6Li in a magnetic field is shown in Figure 3, and a

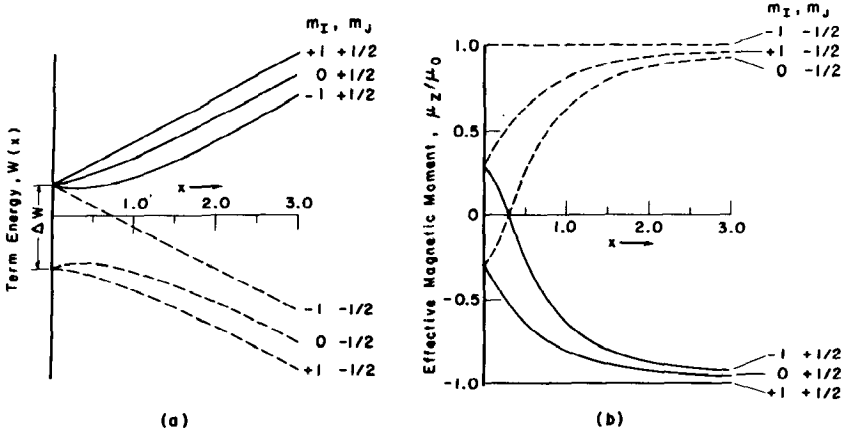

Figure 3 Energy levels and magnetic moments of ^6Li (nuclear spin $I = 1$) in the ground $^2S_{1/2}$ atomic state as a function of magnetic field H, where m_J, m_I are the electronic and nuclear magnetic quantum numbers, and $x = (g_J - g_I)\mu_0 H/\Delta W$ in which g_I and g_J are the nuclear and electronic g values, μ_0 is the Bohr magneton, and $\Delta W = h\Delta\nu$ is the hyperfine structure interval.

schematic diagram of the source in Figure 4. An intense atomic beam of ^{6}Li atoms in its ground state is formed by heating ^{6}Li in an oven with an orifice and by collimating the resulting flux of atoms. The sixpole magnet with its strong inhomogeneous magnetic field transmits only atoms with electronic magnetic quantum number $m_j = +1/2$, which then pass adiabatically into the ionization region where there is a longitudinal magnetic field of about 200 G provided by the polarizing coil. Intense light in the UV range from 1700 to 2300 Å is produced by a vortex-stabilized argon flash lamp and is focussed onto the polarized ^{6}Li atomic beam. The resulting photoelectrons are extracted from the ionization region with a kinetic energy of about 70 keV, and then transported either into the accelerator or into the polarization analyzer that employs double Mott scattering. The electron beam is longitudinally polarized either parallel or antiparallel to the beam direction depending on the direction of the current in the polarizing coil. The operating characteristics of the resulting high energy polarized electron beam are given in Table 1.

The intensity of the high energy polarized electron beam is less by a factor of about $\sim$400 than that of an unpolarized electron beam at SLAC, but because of radiation damage of the polarized target (see below) its intensity is appropriate for polarized e-p scattering.

The electron polarization from the source at 70 keV was measured to an accuracy of 5% by double Mott scattering in which the first scattering at 90° converts the longitudinal polarization to transverse polarization.

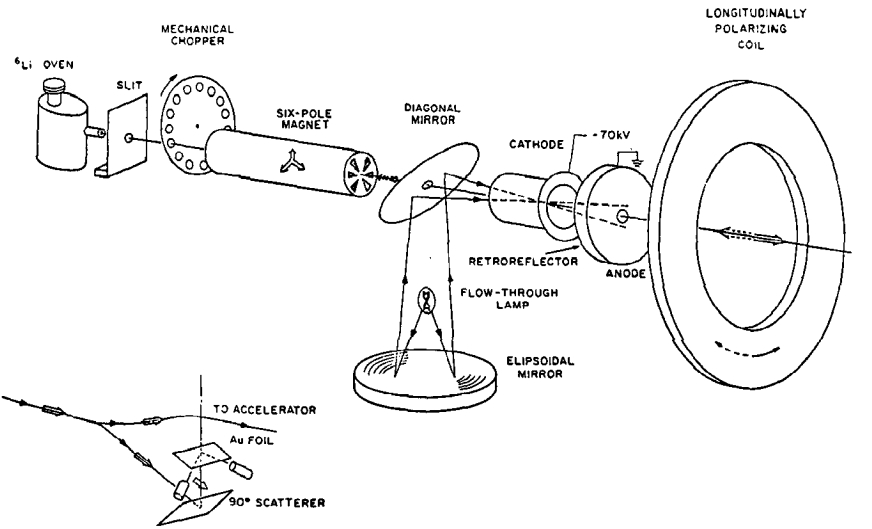

Figure 4 Schematic diagram of PEGGY I showing the principal components of the lithium atomic beam, the UV optics, the ionization region electron optics, and the double Mott scattering polarization analysis.

Table 1 Operating characteristics of polarized electron beam

Characteristic	Value
Pulse length	1.5 μs
Repetition rate	180 pps
Average intensity at GeV energies	5×10^8 e^- per pulse
Pulse-to-pulse intensity variation	$< 5\%$
Polarization	0.80 ± 0.03
Polarization reversal time	3 s
Intensity difference upon reversal	$< 5\%$

After acceleration in the linear accelerator to GeV energies, the longitudinal polarization was measured by elastic electron-electron scattering (Möller scattering) from a magnetized iron foil (60). Möller scattering is an attractive method for measuring the electron polarization at high energy because the cross section and analyzing power are large and the process is purely quantum electrodynamic. Figure 5 shows the Möller asymmetry and laboratory cross section at the representative beam energy of 9.71 GeV. The longitudinal beam polarization P measured as a function of beam energy E is shown in Figure 6. The variation of P with E is caused by the $g-2$ precession of the spin relative to the momentum in the beam switchyard, where the beam from the accelerator is bent by 24.5° into the experimental area. The accuracy with which the longitudinal electron polarization has been determined in the experiments with polarized electrons is about 4%. The error is due to the statistical counting error in the measured asymmetry, uncertainty in the background subtraction, and uncertainty about the electron spin magnetism of the magnetized iron foils.

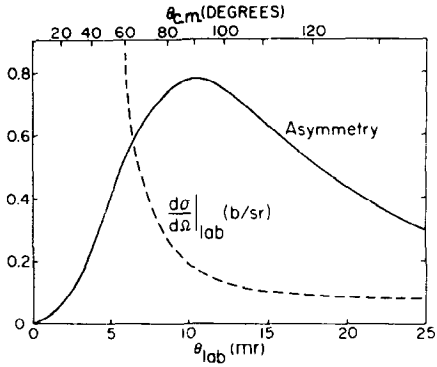

Figure 5 The Möller asymmetry and laboratory cross section plotted versus laboratory angle for the incident electron energy of 9.712 GeV.

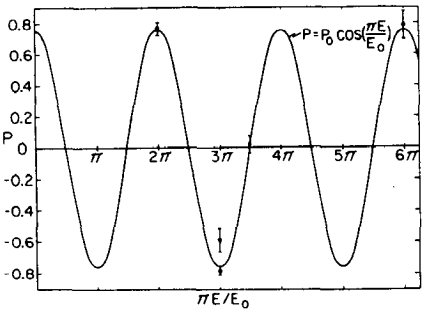

Figure 6 The longitudinal component, P, of the beam polarization plotted versus $\pi E/E_0$, the angle through which the spin precesses relative to the momentum during the 24.5° bend into the experimental area. E is the beam energy and $E_0 = 3.237$ GeV. The curve shown is a best fit to the data and has an amplitude $P_0 = 0.76 \pm 0.03$. P_0 is the only free parameter.

The polarized proton target used is based on the well-known method of dynamic nuclear orientation using a hydrocarbon (butanol) sample with a paramagnetic dopant (porphyrexide) (61–64). Its principal special feature has been the large energy dissipation in the target due to the relatively intense electron beam and the associated damage to the target. Techniques for rastering the beam over the target area in order to minimize the effect of radiation and provide uniform target polarization, for annealing radiation damage, and for rapid changing of target material have been developed. The target operates at 1 K and used a 50-kG magnetic field. A drawing of the target assembly is shown in Figure 7 and the operating characteristics of the target are given in Table 2.

The asymmetries measured in polarized e-p scattering are small. If we designate the experimental counting rate asymmetry by Δ, then we can write

$$\Delta = \frac{N(+)-N(-)}{N(+)+N(-)} = P_e P_p F A \qquad 39.$$

in which $N(+)$ and $N(-)$ designate the scattered electron counts from a polarized proton target of electrons with + and − helicity, respectively. P_e is the polarization of the electron beam, P_p is the polarization of free protons (i.e. those associated with hydrogen) in the target, F is the fraction of scattering events from the target that arise from the free (polarizable) protons, and A is the intrinsic asymmetry associated with polarized e-p scattering. Measurements have shown that $A \simeq 0.2$, in agreement with an early prediction from the Bjorken sum rule. Practically realizable values for P_e, P_p, and F are $P_e \simeq 0.8$m $P_p \simeq 0.6$, and $F \simeq 0.1$. Hence the predicted size of Δ is about 0.01.

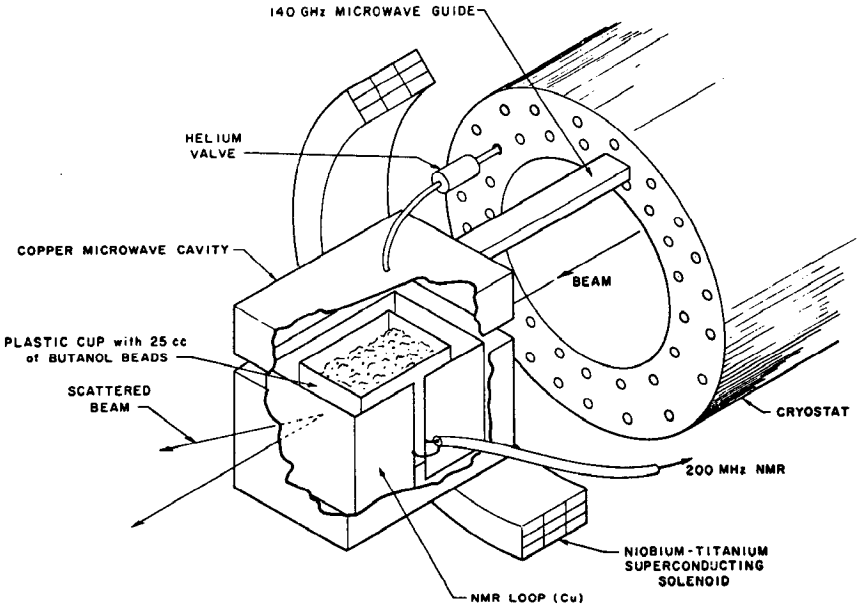

Figure 7 Schematic diagram of the Yale-SLAC polarized proton target operating at 1 K and 50 kG.

The small values of Δ to be measured require careful measurement and control of the intensity, position, and direction of the incident electron beam in order to assure that no false asymmetries are associated with reversal of the helicity of the electron beam.

The electron beam from the accelerator was momentum-analyzed by a transport system whose absolute momentum calibration was $\sim 0.1\%$ and a momentum slit in the transport system limited the beam spread to $\pm 0.375\%$. The electron beam charge per pulse was monitored with two precision toroidal charge monitors. Several sensitive microwave beam

Table 2 Operating characteristics of polarized proton target

Characteristic	Value
Magnetic field (superconducting)	50 kG
Temperature	1 K
Target material	25 cm^3 of butanol-porphyrexide
Maximum polarization, P_p	0.75
Depolarizing dose (1/*e*)	3×10^{14} e^- cm^{-2}
Polarizing time (1/*e*)	~ 4 min
Anneal or target change time	~ 45 min

position monitors located along the beam line from the accelerator output to the target, together with a computer-controlled feedback system including steering magnets and accelerator klystons, controlled the position, angle, and energy of the electron beam incident on the target so that false asymmetries were maintained below 10^{-4} and hence were negligibly small (11, 65).

The scattered electrons were detected and their momentum and scattering angle were measured. In the first experiment (E80) the SLAC 8-GeV spectrometer was used (26, 31, 63). Electron identification was achieved with a gas threshold Čerenkov counter, a 3.25-radiation-length-thick, lead-glass, counter array that sampled the buildup of the electromagnetic shower, and a lead-Isolite shower counter. Less than one pion in 10^3 was misidentified as an electron by this system. An on-line XDS 9300 computer monitored the experiment and recorded data on magnetic tape.

In the second experiment (E130) (11, 65) a new larger acceptance spectrometer was used (see Figure 8). It utilizes two large dipole magnets (B201 and B81) and a detector system consisting of a 1-m diameter × 4-m long N_2 gas Čerenkov counter, a 4000-wire PWC system, a hodoscope, and a segmented lead-glass shower counter. The spectrometer may cover momenta up to 18 GeV/c, and its acceptance $\int d\Omega\, dp/p$ is 0.3 msr with the total momentum acceptance $\Delta p/p$ being about 50%. The momentum resolution $\delta p/p$ of the spectrometer is better than $\pm 1\%$.

The kinematic points at which data have been obtained are shown in Figure 9 and include elastic, resonance region, and deep inelastic points.

The intrinsic e-p asymmetry A is obtained from the measured values of Δ using Equation 39. The measured values of P_e and P_p are used. The quantity F is taken to be the ratio of the number of free protons to the total number of nucleons, corrected for the measured ratio of the neutron to proton scattering cross sections at the kinematic point (66). Radiative corrections to the values of A so obtained are then made using the extensive data

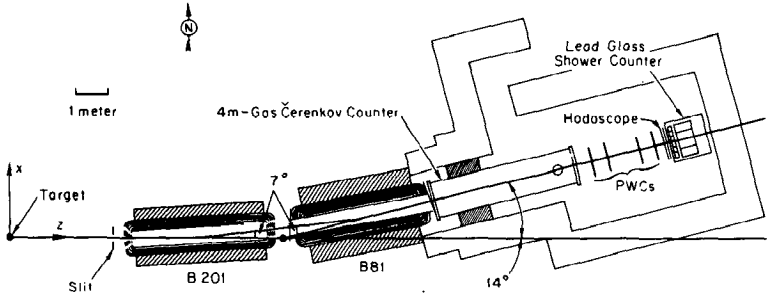

Figure 8 Spectrometer used in SLAC E130 experiment.

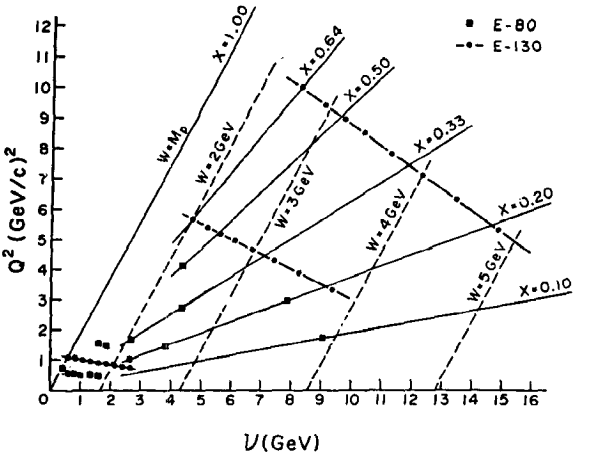

Figure 9 Kinematic points measured.

available on the spin-averaged cross sections, measured values of A, and the calculated values of A for elastic scattering. The equivalent radiator method in the peaking approximation was employed in a self-consistent type of calculation (31, 67, 68). The radiative corrections contribute only a small change in the A values but do increase the statistical errors by about 20–70%. Table 3 shows some typical data.

Exploratory measurements were made of the asymmetry in resonance region scattering (30). Data were obtained at $Q^2 = 0.5$ and 1.5 $(\text{GeV}/c)^2$ in the missing-mass range $W = 1.1$ to 1.9 GeV (see Figure 10).

Table 3 Data sample from SLAC E130 ($E = 22.659$ GeV; $\theta = 10°$)

x	Q^2	ν	W	Δ	A^a	A^b	A/D^b
0.19	5.32	14.93	4.85	0.030(0.009)	0.439(0.137)	0.461(0.163)	0.69(0.24)
0.25	6.32	13.47	4.45	0.017(0.003)	0.248(0.049)	0.263(0.056)	0.44(0.09)
0.31	7.14	12.28	4.09	0.020(0.003)	0.279(0.047)	0.289(0.053)	0.53(0.10)
0.37	7.83	11.28	3.77	0.026(0.004)	0.358(0.054)	0.366(0.060)	0.74(0.12)
0.43	8.41	10.43	3.46	0.021(0.005)	0.288(0.064)	0.294(0.070)	0.65(0.16)
0.49	8.92	9.70	3.18	0.020(0.006)	0.257(0.085)	0.261(0.094)	0.62(0.22)
0.55	9.35	9.06	2.92	0.018(0.009)	0.288(0.118)	0.231(0.124)	0.60(0.32)
0.64	9.91	8.25	2.54	0.017(0.010)	0.212(0.126)	0.214(0.131)	0.61(0.38)

[a] Measured values without radiative correction (total errors in parentheses).
[b] Relatively corrected values (total errors in parentheses).

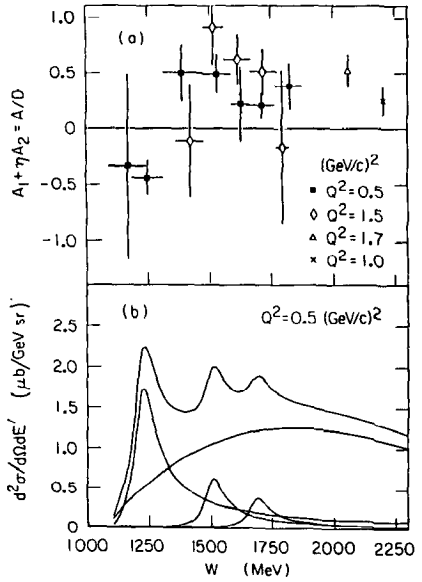

Figure 10 (*a*) Asymmetry vs missing-mass W. (*b*) Differential cross section vs W. Also shown is a decomposition into individual resonances and the background.

4. COMPARISON OF THEORY AND EXPERIMENT

For elastic scattering the theoretical value of the asymmetry in the one-photon exchange approximation (68) is given by

$$A = \frac{\tau G_M}{G_E}\left\{\frac{2M}{E} + \frac{G_M}{G_E}\left[\frac{2\tau M}{E} + 2(1+\tau)\tan^2\frac{\theta}{2}\right]\right\} \times \left\{1+\tau\left(\frac{G_M}{G_E}\right)^2\left[1+2(1+\tau)\tan^2\frac{\theta}{2}\right]\right\}^{-1} \quad 40.$$

in which $\tau = Q^2/4M^2$, $q^2 = -Q^2 = -4EE'\sin^2(\theta/2)$ is the square of the four-momentum of the virtual photon, M is the proton mass, E' is the scattered electron energy, and G_E and G_M are the electric and magnetic elastic form factors of the proton. The electron mass has been neglected. The measurement of A for elastic scattering was chosen primarily to test the validity of the experimental method. Alternatively, we can regard the measurement as a test of Equation 41 and as a determination of the sign of G_E/G_M. The experimental value of A is 0.103 ± 0.015, in reasonable agreement with the theoretical value $A = 0.112 \pm 0.001$ (63).

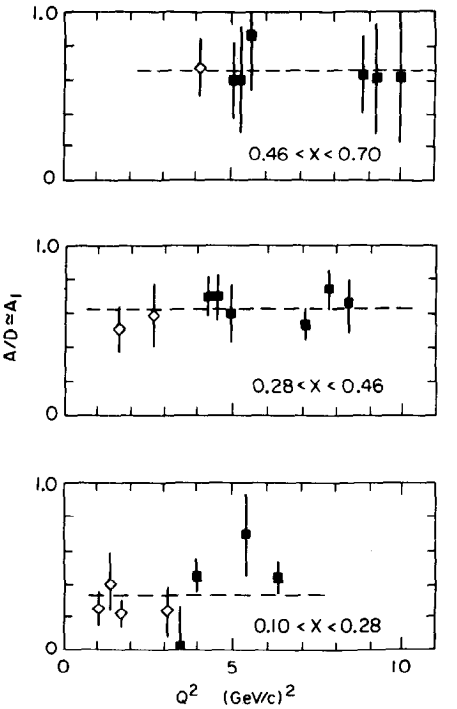

Figure 11 Radiatively corrected values of $A/D \simeq A_1$ obtained in SLAC E80 (*open diamonds*) and SLAC E130 (*closed squares*).

For deep inelastic scattering Figure 11 shows values of $A/D \simeq A_1$ obtained from experiments E80 and E130 plotted vs Q^2 in three intervals of x (26, 36, 65). The error bars include statistical and systematic errors. To test scaling of A_1 the values A/D have been divided by $\sqrt{x}$ (which described well the x dependence of the Q^2-combined data) and least-squares straight lines have been fit in the region $Q^2 > 2$ GeV^2. The assumption of scaling (zero slope) gives χ^2/DOF of 0.43/5, 2.4/5, and 5/3, and confidence levels of 99%, 80%, and 18%, for the top, middle, and bottom boxes, respectively. We therefore conclude that scaling of A_1 holds within errors. The Q^2-combined values of A/D are shown in Figure 12. The data are best described by $A/D = (0.94 \pm 0.08)\sqrt{x}$ (with χ^2/DOF = 9.5/11).

The data permit a test of the Ellis-Jaffe sum rule (40) for the proton

$$S_{BJ}^p = 2\int_0^1 g_1^p \, dx = \int_0^1 \frac{dx}{x} \frac{A_1^p F_2^p}{1+R^p} \frac{(0.89)}{3} = 0.372 \pm 0.002 \qquad 41.$$

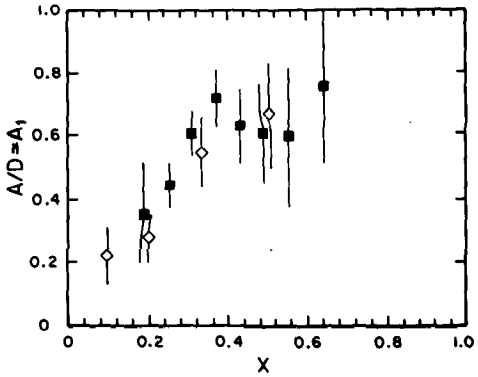

Figure 12 Measured values of A/D vs x. Points were obtained from Figure 11 data assuming A/D values are independent.

and of the Bjorken sum rule (12, 14)

$$S_{Bj} = 2\int_0^1 (g_1^p - g_1^n)\,dx = \int_0^1 \frac{dx}{x}\left(\frac{A_1^p F_2^p}{1+R^p} - \frac{A_1^n F_2^n}{1+R^n}\right)$$

$$= \frac{1}{3}\left|\frac{g_A}{g_V}\right| = 0.418 \pm 0.002 \qquad 42.$$

if A_1^n is approximated by zero. The integrand $A_1^p F_2^p/(1+R^p)$ is plotted in Figure 13 using $F_2^p(x, Q^2)$ from available data and the value $R = 0.25 \pm 0.10$ from the SLAC e-p data. The smooth curve in the region $0.1 < x < 0.64$ is obtained from our fit $A_1 = 0.94\sqrt{x}$ and F_2^p evaluated at $Q^2 = 4\ (\mathrm{GeV}/c)^2$ (which is the mean Q^2 value of our data). The integral under this curve in the data region $0.1 < x < 0.64$ is 0.189 ± 0.016, which saturates 45% of the

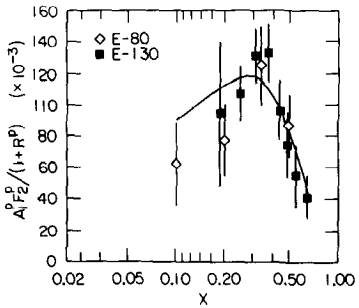

Figure 13 Experimental values of $A_1^p F_2^p/(1+R^p)$. F_2^p and R are from unpolarized data. The smooth curve is obtained using $A_1^p(x) = 0.94\sqrt{x}$.

Bjorken sum rule. The integral over the full x range using the Regge theory prediction $A_1 \propto x^{1.14}$ for $x < 0.01$ and our fit $A_1 = 0.94\sqrt{x}$ for $x < 0.1$ gives

$$2\int_0^1 g_1^p(x)\,dx = 0.33 \pm 0.10.$$

In conclusion, our result is consistent with the Ellis-Jaffe sum rule for the proton. This implies that our results are also consistent with the Bjorken sum rule provided that the neutron contribution is as small as suggested by the Ellis-Jaffe sum rule for the neutron.

Comparison of our data on A_1^p with theoretical values provides a major test for our understanding of nucleon structure. The generally accepted theory of quantum chromodynamics involving quarks and gluons has not yet been successfully applied from its own first principles to calculate either spin-independent or spin-dependent structure functions. However, perturbative QCD does make some important predictions about nucleon structure functions including A_1 for x near 1, which is the high momentum tail of the wave function. The models of nucleon structure picture the proton as consisting of three valence quarks, two u quarks and a d quark, together with gluons and a sea of quark-antiquark pairs. They picture the neutron as two d quarks and a u quark together with gluons and the sea. The early models assumed SU(6) symmetry for the wave function. However, experimental data on F_2^n/F_2^p (69) and on A_1^p at large x required that SU(6) symmetry breaking be introduced. The important and unsymmetrical aspect of the wave function for the proton (neutron) near $x = 1$, which is predicted by perturbative QCD, is the occurrence with high probability of a single u (d) quark with large x and a diquark with isotopic spin $I = 0$ and spin component $S_z = 0$ (27–29). Of the various models for the proton wave function that are intended to represent the nonperturbative QCD solution, perhaps the most basic is the MIT bag model (70), which incorporates confinement.

A comparison of our data on $A_1^p(x)$ with various model predictions is shown in Figure 14. We should remark that some earlier nonquark models of the proton predicted negative values for A_1, but all quark models predict that A_1 is positive. Hence the earliest data indicating that A_1 is positive provided a crucial test of the quark model (26). In the quark model A_1 can be written (71)

$$A_1(x) = \frac{\sum_i e_i^2[f_i^{\uparrow} - f_i^{\downarrow}]}{\sum_i e_i^2[f_i^{\uparrow} + f_i^{\downarrow}]} \qquad 43.$$

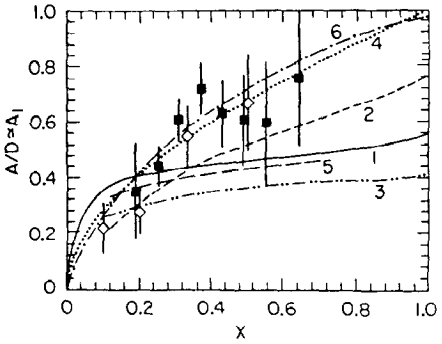

Figure 14 Experimental values A_1 compared with theories. 1. Symmetrical valence-quark model (18). 2. Current quarks (44). 3. Orbital angular momentum (39, 49). 4. Unsymmetrical model (45, 46). 5. MIT bag model (51, 70). 6. Source theory (72).

in which the sum is over the quarks i, e_i is the charge of the ith quark, and $f^{\uparrow}_i$ ($f^{\downarrow}_i$) is the probability for quark i to have its spin parallel (antiparallel) to the target nucleon spin. A_1 clearly provides a measure of the probability that the quark spins are aligned with the nucleon spin. Our data are consistent only with the Carlitz-Kaur (45, 46), the Schwinger (72), and possibly the Close (44) models of A_1. Our confidence levels in these models are 70%, 70%, and 3%, respectively. Curve 4 of Figure 14 provides an unsymmetrical model of the quark distributions involving SU(6) breaking, Regge theory at small x, the Melosh transformation (73), and agreement, with the Bjorken sum rule. Curve 6 is based on Schwinger's source theory (72), which is not a quark model.

For resonance region scattering, the measured asymmetries A/D are predominantly large and positive throughout the entire range in missing mass W except in the region of the $\Delta(1232$ MeV) resonance, where A/D is expected to be negative because of magnetic dipole excitation. In principle the measured asymmetry values can be predicted from a multipole analysis of complete but unpolarized electroproduction data (74). Figure 15 displays the predictions based on a multipole analysis of single-pion electroproduction data only, which accounts for about half of the differential cross section. The agreement between these predictions and the data is rather good, and hence indicates that the net asymmetry contributed by channels other than single-pion production cannot be very different from the measured asymmetries. Figure 16 indicates that scaling applies for the resonance region data except at the $\Delta(1232)$ point, and hence that the spin-dependent behavior is also consistent with a global duality mechanism in analogy to the unpolarized case.

It is well known in the theory of atomic hyperfine structure that a

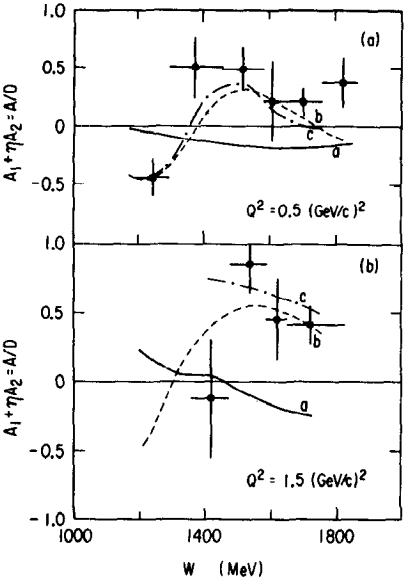

Figure 15 (*a*) Asymmetry data is $Q^2 \simeq 0.5$ (GeV/c)^2 compared with a multipole analysis performed by Devenish & Lyth (74): curve *a*, Born term alone; curve *b*, Born terms plus $\Delta(1232)$; and curve *c*, Born terms plus all resonances. (*b*) Same for $Q^2 \simeq 1.5$ (GeV/c)^2.

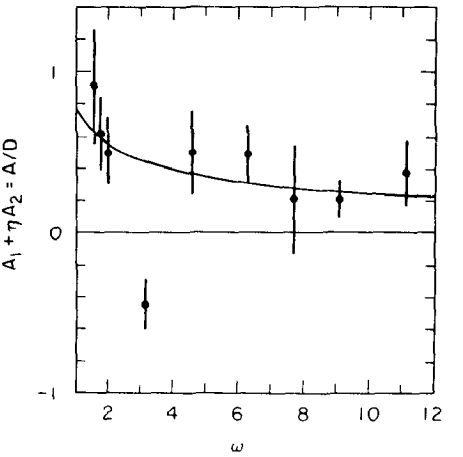

Figure 16 Asymmetry vs scaling variable ω. The curve $0.7\omega^{-1/2}$ is a fit to deep inelastic data ($W > 2$ GeV). The data points are the resonance region results ($W < 2$ GeV).

significant contribution to the hyperfine splitting interval $\Delta\nu$ in hydrogen arises from the spin-dependent polarizability of the proton. Figure 17 gives the experimental and theoretical values for $\Delta\nu$. The contribution of the spin-dependent polarizability is designated $\delta_p(\text{pol})$. The principal theoretical uncertainty in $\Delta\nu$ is due to $\delta_p(\text{pol})$, for which a positivity bound $|\delta_p(\text{pol})| \lesssim 4$ ppm has been calculated (33, 34). The quantity $\delta_p(\text{pol})$ can be expressed in terms of the spin-dependent structure functions G_1 and G_2, which are measured in polarized e-p scattering. The greatest contribution to $\delta_p(\text{pol})$ comes from the small-Q^2 region, including the proton resonances. The experimental data available to date support the theoretical estimates of $\delta_p(\text{pol})$. However, considerably more data are needed to provide a significant quantitative determination of $\delta_p(\text{pol})$.

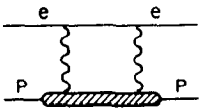

$$\Delta\nu_{\text{expt.}} = 1\,420\,405\,751.766\ 7(10)\ \text{Hz}$$

$$\Delta\nu_{\text{theory}} = \Delta\nu_F(1+\delta_{\text{QED}}+\delta_p) \qquad \Delta\nu_F = \text{Fermi value};\ \delta_{\text{QED}} = \text{QED corrections}$$
$$\delta_p = \text{Proton recoil and structure term}$$

$$\delta_p = \delta_p(\text{rigid}) + \delta_p(\text{polarizability}) = -34.6(9) \times 10^{-6} + \delta_p(\text{pol})$$

$$\delta_p(\text{pol}) = \frac{\alpha}{\pi}\frac{m_e}{M}\frac{1}{2(1+\mu_A)}\int_0^\infty \frac{d(-q^2)}{(-q^2)}\left[\Delta_1(q^2)+\Delta_2(q^2)\right]$$

$$\Delta_1(q^2) = \frac{9}{4}\left[F_2(q^2)\right]^2 + 5M^3\int_{\nu_1(q^2)}^\infty \frac{d\nu}{\nu}\beta_1\left(\frac{\nu^2}{-q^2}\right)G_1(\nu,q^2)$$

$$\Delta_2(q^2) = 3M^2\int_{\nu_1(q^2)}^\infty \frac{d\nu}{\nu^2}\beta_2\left(\frac{\nu^2}{-q^2}\right)q^2\,G_2(\nu,q^2)$$

$$\beta_1(x) \equiv \frac{4}{5}\left(-3x+2x^2+2(2-x)\sqrt{x(1+x)}\right);\ \beta_2(x) \equiv 4x\left(1+2x-2\sqrt{x(1+x)}\right)$$

$$F_2(q^2) = \text{Pauli form factor};\ F_2(0) = \mu_A;\ \nu_1(q^2) = m_\pi + \frac{(m_\pi^2 - q^2)}{2M}$$

Figure 17 Hyperfine structure interval $\Delta\nu$ in hydrogen. The Feynman diagram and the expression given for $\delta_p(\text{pol})$ indicate the contribution to $\Delta\nu$ of the spin-dependent polarizability of the proton.

5. FUTURE PROSPECTS

On the experimental side only a modest amount of data on polarized e-p scattering have been obtained, primarily because of the difficulty of the experiment. However, major advances in our knowledge are certainly possible both with polarized electron and with polarized muon scattering from polarized nucleon targets.

Thus far essentially only the spin-dependent structure function A_1^p has been measured. Actually the intrinsic e-p asymmetry $A = D(A_1 + \eta A_2)$ has been determined, but for the kinematics of scattering longitudinally polarized electrons by longitudinally polarized protons the kinematic term η is relatively small so that $A \simeq DA_1$. Determination of A_2 can be done with the protons polarized transverse to the incident longitudinally polarized electron beam. For this case the measured asymmetry $A_T = d(\zeta A_1 - A_2)$ and the kinematic factor ζ is relatively small so that, with measurements of both A and A_T, both A_1 and A_2 can be determined.

The spin-dependent structure functions for the neutron, A_1^N and A_2^N, can also be determined using a polarized deuteron target with both longitudinal and transverse polarizations, as well as a polarized proton target. In first approximation an appropriate subtraction of proton from deuteron data provides the information on the neutron. Effects of the deuteron binding and of the admixture of $^3D_1$ state in the deuteron wave function are estimated to be small but must also be considered.

A proposal (75) was submitted to SLAC (E138) to do these measurements using recent advances in the technology of polarized electron beams and polarized targets. For many years the material used in a polarized target has been a hydrocarbon chemically doped with a paramagnetic substance. Recently it has been found (76–78) that NH_3 and ND_3 after irradiation in a high energy electron (or parton) beam can be successfully dynamically polarized. The resulting polarized target has a significantly higher fraction of polarizable protons than a hydrocarbon and also has ~ 30 times the resistance to radiation. With the irradiated NH_3 it is then advantageous to use the higher intensity GaAs polarized electron source, despite its lower polarization as compared to the atomic ^{6}Li source.

Within less than two years the CERN European Muon Collaboration plan to measure polarized μ-p scattering using a longitudinally polarized muon beam with energies up to about 250 GeV and a longitudinally polarized proton target 1 m in length. The kinematic range for the scattering will extend up to $Q^2 \simeq 60$ (GeV/c)^2 with $0.1 \lesssim x \lesssim 0.7$. The muon beam at Fermilab from the Tevatron with energies up to 700 GeV can also be considered for polarized μ-p scattering experiments. Extensive

measurement of asymmetries in the resonance region can be done with lower energy polarized e^- beam in the several GeV range, e.g. with SLAC or Bonn beams or with the planned 4-GeV CW National Accelerator in the US.

Knowledge of the neutron spin-dependent asymmetry A_1^N is necessary for a test of the Bjorken polarization sum rule. Several theoretical predictions of A_1^N have been made on the basis of models of nucleon structure and are shown in Figure 18. The SU(6) relativistic symmetric valence-quark model of the neutron predicts that $A_1^N = 0$ for all x. The other models also predict that A_1^N is small for $x < 0.5$. The unsymmetrical model, which fits well the measured A_1^p values, incorporates the perturbative QCD prediction that $A_1^N \to 1$ as $x \to 1$, when the single d or u quark with high x carries the entire spin component of the nucleon.

The asymmetry A_2 arises from an interference between amplitudes for absorption of virtual longitudinal and transverse photons by the proton. There is a sum rule related to A_2 (41). In the scaling limit simple parton models predict that A_2 becomes zero, and there is a positivity bound $|A_2|$

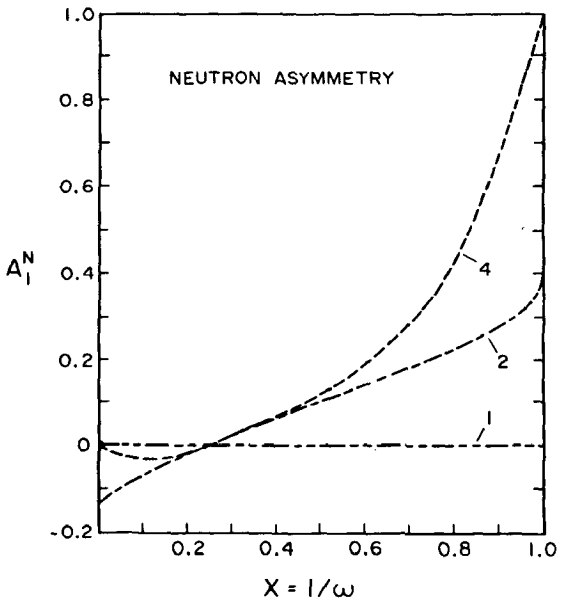

Figure 18 Theoretical predictions for A_1 (neutron). The models are as follows: 1. a relativistic symmetric valence-quark model of the neutron (18), 2. a model incorporating the Melosh transformation, which distinguishes between constituent and current quarks; 4. an unsymmetrical model in which the entire spin of the neutron is carried by a single quark in the limit of $x = 1$.

$< R^{1/2}$. Physically A_2 arises from quark masses and quark transverse momenta. Figure 19 shows various theoretical predictions for A_2 for the kinematics of the proposed E138 experiment. The positivity limit of $|A_2| < R^{1/2}$ is 0.5, since the best current value of R in this kinematic range is $R = 0.25 \pm 0.10$. Parenthetically, this large experimental value for R, which is expected theoretically to be zero in the scaling limit poses a problem for QCD theory, which may be related to higher-twist terms; the comparison of theory and experiment for A_2 can be expected to pose a similar problem. In addition Figure 19 shows the prediction of the MIT bag model and a prediction given from $g_2(x) = 0$ that is consistent with SU(6). Data on A_2 are important for comparison with these and other theories for A_2. In addition, data on A_2 are important to the experimental determination of A_1, since we measure $A/D = A_1 + \eta A_2$, and we only obtain a value of A_1 provided ηA_2 is sufficiently small. With the positivity bound for A_2, the value of ηA_2 for E80-E130 data is between 0.2 and 0.8 times the experimental one-standard-deviation error in the determination of A/D.

A major experiment is planned to be run at CERN by the European Muon Collaboration in 1984 (79) to measure the asymmetry in deep inelastic scattering of longitudinally polarized muons by longitudinally polarized protons. A significant test of the predicted scaling of the spin-dependent structure function A_1^p will be obtained from this CERN data at high Q^2 [$Q^2 \leq 60$ (GeV/c)^2] and the SLAC data with $2 < Q^2 < 10$ (GeV/c)^2. Indeed the proton data to be obtained in the proposed experiment will be more precise than that obtained in E130 (by a factor of 2 to 3), and hence useful for the test of scaling. Figure 20 gives a theoretical prediction of scaling violation using $\Lambda = 0.1$ and 0.4 GeV.

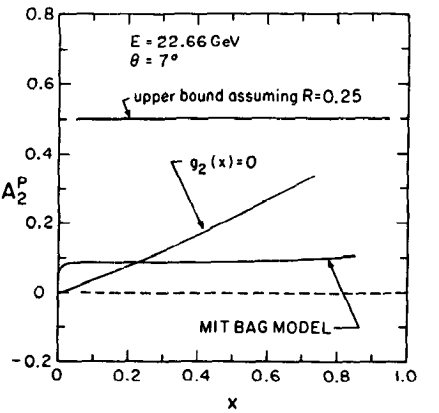

Figure 19 Theoretical predictions for A_2 (proton) for the kinematics of the E138 proposal.

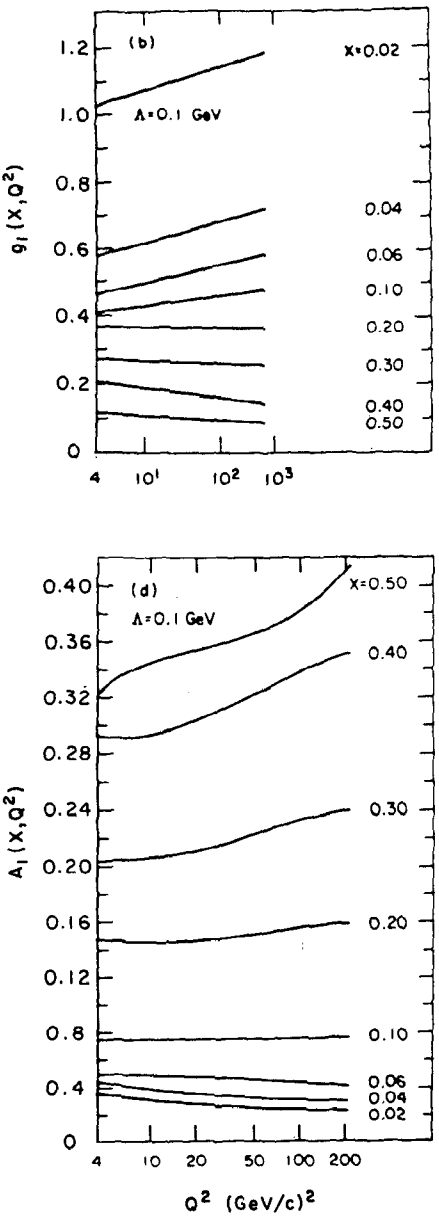

Figure 20 (*Top*) Scaling violation of $g_1(x, Q^2)$ (23) for two values of Λ, obtained by QCD and a broken SU(6) model (44) at $Q_0 = 2$ GeV. (*Bottom*) Scaling violations of $A_1(x, Q^2)$ obtained from (*top*) and known values of $F_1(x, Q^2)$.

Finally we emphasize that knowledge of the internal spin structure of the nucleon, apart from its importance to our understanding of nucleon structure, is essential to the interpretation of spin-dependent high energy phenomena involving hadrons (80–83). These include hadron-hadron scattering, the polarized Drell-Yan process, and production of polarized W or Z vector bosons in collisions of polarized protons in a high energy storage ring.

In conclusion, we wish to emphasize that the polarization data in deep inelastic electron (muon) scattering from polarized nucleons has proven to be very important for our understanding of the nucleon structure. During the years a consistent and remarkably simple picture of the nucleon has been emerging from experimental information and from QCD as the theoretical guidance to organize the observations. Accordingly, the nucleon as an extended object (with form factors and resonance excitations) is best described in terms of three permanently bound constituent quarks. The bound constituent quarks appear to deep inelastic probes as an almost free parton distribution with three valence quarks and a cloud of quark-antiquark pairs and gluons. The spin structure of the nucleon from the wave function of the constituent quarks is inherited in the spin distribution of partons. The aim of deep inelastic polarization experiments is to explore and understand this parton spin distribution in our general investigation of the nucleon structure. The first polarization experiments were remarkably successful. They clearly established the quark spin connection. Further polarization experiments on the neutron would improve significantly our present understanding of the nucleon structure.

ACKNOWLEDGMENT

This work was supported in part by the US Department of Energy under Contract No. DE-AC02-76ERO3075. One of us (JK) would like to acknowledge the kind hospitality extended to him from the Institute for Theoretical Physics of the University of California, Santa Barbara.

Literature Cited

1. Altarelli, G. 1982. *Phys. Rep.* 81(1): 1–127
2. Itzykson, C., Zuber, J. B. 1980. *Introduction to Quantum Field Theory.* New York: McGraw-Hill. 705 pp.
3. Marciano, W., Pagels, H. 1978. *Phys. Rep.* 36C: 137
4. Wilczek, F. 1982. *Ann. Rev. Nucl. Part. Sci.* 32: 177
5. Gell-Mann, M. 1964. *Phys. Lett.* 8: 217
6. Adler, S. L., Dashen, R. F. 1968. *Current Algebra and Applications to Particle Physics.* New York: Benjamin. 394 pp.
7. Wilson, K. G. 1971. *Phys. Rev.* D3: 1818
8. Fritzsch, H., Gell-Mann, M. 1972. *XVI Int. Conf. on High Energy Physics, Proc.*, Vol. II, p. 135
9. Gross, D. J., Wilczek, F. 1973. *Phys. Rev. Lett.* 30: 1343

10. Politzer, H. D. 1973. *Phys. Rev. Lett.* 30:1346
11. Hughes, V. W., et al. 1981. In *High Energy Physics with Polarized Targets*, ed. C. Joseph, J. Soffer, p. 331. Lausanne: Berkhauser Verlag.
12. Bjorken, J. D. 1966. *Phys. Rev.* 148:1467
13. Galfi, L., et al. 1970. *Phys. Lett.* 31B:465
14. Bjorken, J. D. 1970. *Phys. Rev.* D1:465
15. Kuti, J. 1972. *Proc. Neutrino '72*, ed. G. Marx, A. Frenkel, Vol. 2, p. 101
16. Galfi, L., et al. 1972. *Acta Phys. Hungarica* 21:85
17. Hey, A. J. G., Mandula, J. E. 1972. *Phys. Rev.* D5:2610
18. Kuti, J., Weisskopf, V. W. 1971. *Phys. Rev.* D4:3418
19. Feynman, R. P. 1969. *Phys. Rev. Lett.* 23:1415
20. Bjorken, J. D., Paschos, E. A. 1969. *Phys. Rev.* 185:1975
21. Feynman, R. P. 1972. *Photon-Hadron Interactions*. Reading: Benjamin
22. Kodaira, J., et al. 1979. *Phys. Rev.* D20:627
23. Darrigol, O., Hayot, F. 1978. *Nucl. Phys.* B141:391
24. Matsuda, S., Uematsu, T. 1980. *Nucl. Phys.* B168:181
25. Kodaira, J. 1980. *Nucl. Phys.* B169:181
26. Alguard, M. J., et al. 1976. *Phys. Rev. Lett.* 37:1261
27. Feynman, R. P. 1972. *Proc. Neutrino '72*, Vol. II, p. 75
28. Brodsky, S. J. 1981. See Ref. 11, p. 169
29. Farrar, G., Jackson, D. 1975. *Phys. Rev. Lett.* 35:1416
30. Baum, G., et al. 1981. *Phys. Rev. Lett.* 45:2000
31. Alguard, M. J., et al. 1978. *Phys. Rev. Lett.* 41:70
32. Iddings, C. K. 1965. *Phys. Rev.* 138B:446
33. Gnädig, P., Kuti, J. 1972. *Phys. Lett.* 42B:241
34. de Rafael, E. 1971. *Phys. Lett.* 37B:201
35. Gilman, F. 1973. *Proc. SLAC Summer Inst. on Part. Phys.*, Vol. I, p. 71
36. Hey, A. J. G. 1974. *Daresbury Lect. Note Ser.*, No. 13
37. Doncel, M. G., de Rafael, E. 1971. *Nuovo Cimento* 4A:363
38. Gnädig, P., Niedermayer, F. 1973. *Nucl. Phys.* B55:612
39. Sehgal, L. M. 1974. *Phys. Rev.* D10:1663
40. Ellis, J., Jaffe, R. 1974. *Phys. Rev.* D9:1444
41. Burkhardt, H., Cottingham, W. N. 1970. *Ann. Phys.* 56:453
42. Heimann, R. L. 1973. *Nucl. Phys.* B64:429
43. Kuti, J. 1982. In *Unified Theories of Elementary Particles*, ed. P. Breitenlohner, H. P. Dürr, p. 90. Berlin: Springer Verlag
44. Close, F. E. 1974. *Nucl. Phys.* B80:269
45. Carlitz, R., Kaur, J. 1976. *Phys. Rev. Lett.* 38:673
46. Kaur, J. 1977. *Nucl. Phys.* B128:219
47. Altarelli, G., et al. 1974. *Nucl. Phys.* B69:531
48. Gourdin, M. 1972. *Nucl. Phys.* B38:418
49. Look, G. W., Fischbach, F. 1977. *Phys. Rev.* D16:211
50. Joshipura, A. S., Roy, P. 1980. *Phys. Lett.* B92:348
51. Hughes, R. J. 1977. *Phys. Rev.* D16:622
52. Domokos, G., et al. 1971. *Phys. Rev.* D3:1191
53. Close, F., et al. 1974. *Nucl. Phys.* B77:281
54. Le Yaouanc, A., Oliver, L., Pène, O., Raynal, J. C. 1975. *Phys. Rev.* D11:680
55. Wandzura, S., Wilczek, F. 1977. *Phys. Lett.* B72:195
56. Brodsky, S. J., Drell, S. D. 1970. *Ann. Rev. Nucl. Sci.* 20:147
57. Kessler, J. 1976. *Polarized Electrons*. Berlin: Springer Verlag
58. Hughes, V. W., et al. 1971. *Phys. Rev.* A5:192
59. Alguard, M. J., et al. 1979. *Nucl. Instrum. Methods* 163:29
60. Cooper, P. S., et al. 1975. *Phys. Rev. Lett.* 34:1589
61. Abragam, A., Goldman, M. 1978. *Rep. Prog. Phys.* 41:395
62. Borghini, M. 1971. *Proc. 2nd Int. Conf. on Polarized Targets*, ed. G. Shapiro, p. 1. Berkeley: Univ. Calif. Press
63. Alguard, M. J., et al. 1976. *Phys. Rev. Lett.* 37:1258
64. Ash, W. W. 1976. *High Energy Physics with Polarized Beams and Targets*, ed. M. L. Marshak, p. 485. New York: Am. Inst. Phys.
65. Baum, G., et al. 1983. *Phys. Rev. Lett.* In press
66. Bodek, A., et al. 1979. *Phys. Rev.* D20:1471
67. Schuler, K. P. 1979. *High Energy Physics with Polarized Beams and Polarized Targets*, ed. G. H. Thomas, p. 217. New York: LAIP
68. Dombey, N. 1969. *Rev. Mod. Phys.* 41:236
69. Buras, A. J., Gaemers, K. H. F. 1978. *Nucl. Phys.* B132:249
70. Jaffe, R. L. 1975. *Phys. Rev.* D11:1953
71. Close, F. E. 1979. *An Introduction to Quarks and Partons*. London: Academic
72. Schwinger, J. 1977. *Nucl. Phys.* B123:223

73. Melosh, H. J. 1974. *Phys. Rev.* D9:1095
74. Devenish, R. C. E., Lyth, D. H. 1975. *Nucl. Phys.* B93:109
75. Hughes, V. W., Schuler, P. K. 1982. *SLAC Proposal E138*
76. Seely, M. L., et al. 1982. *High Energy Spin Physics–1982*, ed. G. Bunce, *AIP Conf. Proc. No. 95*, p. 526
77. Niinikoski, R. O., Rieubland, J.-M., 1979. *Phys. Lett.* 72A:141
78. Hartel, U., et al. 1982. See Ref. 11, p. 453
79. Gabathuler, E. 1974. *CERN EMC Proposal*
80. Baldracchini, F., et al. 1980. *Int. Cent. for Theor. Phys. Trieste Tech. Rep.*
81. Hidaka, K., et al. 1980. *Phys. Rev.* D21:1316
82. Craigie, N., et al. 1980. *Phys. Lett.* B96:381
83. Sivers, D. 1978. *High Energy Physics with Polarized Beams and Polarized Targets*, ed. H. G. Thomas, *AIP Conf. Proc. No. 51*, p. 505

Annual Review of Nuclear and Particle Science
Volume 33, 1983

CONTENTS